Magnetotelluric inversion for 2D anisotropic conductivity structures

Yuguo Li (FU Berlin), Josef Pek (Prag) and Heinrich Brasse (FU Berlin)

Abstract

We report on progress in developing a magnetotelluric inversion method for two-dimensional anisotropic conductivity distribution. A standard two-dimensional model is discretized into a number of rectangular cells, each with a constant conductivity tensor, and the solution of the inverse problem is obtained by minimizing a global objective functional consisting of data misfit, a structural constraint and an anisotropy constraint. All minimizations are carried out by using the Gauss-Newton algorithm, and model perturbations at each iteration step are obtained by a conjugate gradient least squares method. The inversion algorithm is tested on synthetic data generated by two elementary models: a single prism and two prisms with anisotropy.

Keywords: electrical anisotropy, 2D inversion, MT.

1 Introduction

Electrically anisotropic structures have recently gained serious attention in electromagnetic induction studies of the Earth's crust and upper mantle. Complex studies in the KTB area clearly evidenced the real existence of crustal electrical macro-anisotropy that fits well into the tectonic plot of the region (e.g., Eisel & Haak, 1999). Considering jointly the seismic and electric anisotropy in the lithospheric and sub-lithospheric upper mantle has evolved into a promising indicator for large-scale deformation processes in the Earth (e.g., Mareschal *et al.*, 1995; Simpson, 2001; Bahr & Simpson, 2002). As two-dimensional (2D) anisotropy can produce magnetotelluric (MT) effects analogous to those generated by complex 3D structures with multiple co-acting strikes, anisotropic models may be in suitable cases employed as better tractable surrogates for those difficult 3D settings (e.g., Lezaeta & Haak, 2003; Weckmann *et al.*, 2003).

As compared to the isotropic case, the MT inversion for a generally anisotropic conductivity distribution in 2D laterally inhomogeneous structures has to cope not only with increased number of model parameters (by a factor of six in the most general anisotropic case) and more difficult direct and sensitivity solution procedures (coupled system of quasi-E and quasi-H-equations), but also with a largely more complex pattern of equivalencies and ambiguities of the model parameters within the structure.

At present, we have finalized the very basic steps towards a working 2D MT inversion algorithm for anisotropic conductivities. In a companion paper (Pek *et al.*, this volume), the theoretical and numerical principles of the parametric sensitivity calculations for 2D anisotropic MT models are presented. The authors show two approaches for calculating the parametric sensitivity of MT fields. The first approach directly solves the boundary value problem for the parametric sensitivities by using the finite volume (FV) approximation, the second method exploits the electromagnetic reciprocity principle. The latter approach is more efficient when the number of data sites is less than that of the model parameters used in the inversion. In the present paper, the sensitivity computations that employ the reciprocity principle are incorporated into the inverse procedure for 2D anisotropic conductivity structures and an MT anisotropic inversion method is presented. In what follows, the inversion methodology is described briefly, and the algorithm is then illustrated by inverting data sets for two simple synthetic models.

2 Inversion methodology

2.1 Inversion parameter

The conductivity distribution in an anisotropic medium can be described by a symmetric positive-definite 3×3 conductivity tensor that can be represented by three positive principal conductivities and three Euler angles. It is suitable to choose the logarithms of three principal conductivities (σ_1, σ_2, and σ_3) and three Euler angles (α_s, α_d, and α_l) as inversion parameters. For a single homogeneous cell in the subsurface, we have thus six inverse parameters, i.e. $\ln \sigma_1$, $\ln \sigma_2$, $\ln \sigma_3$, α_s, α_d, and α_l.

2.2 Objective functional

The objective functional to be minimized is

$$\Phi(\mathbf{m}, \lambda_s, \lambda_a) = \Phi_d(\mathbf{m}) + \lambda_s \Phi_s(\mathbf{m}, \mathbf{m}^{ref}) + \lambda_a \Phi_a(\mathbf{m}), \tag{1}$$

with

$$\Phi_d(\mathbf{m}) = ||\mathbf{W}_d[\mathbf{d}^{mod}(\mathbf{m}) - \mathbf{d}^{obs}]||^2, \tag{2}$$

where λ_s and λ_a are weights of the structure and anisotropy penalties, respectively, $\mathbf{d}^{mod}(\mathbf{m})$ is predicted data for a given model conductivity distribution $\mathbf{m}$, $\mathbf{d}^{obs}$ is the measured data and $\mathbf{W}_d$ is a covariance matrix of the measured data. As the diagonal impedance elements play a crucial role in the inversion for an anisotropic electrical structure, we assume that the measured data vector $\mathbf{d}^{obs}$ consists of the real and imaginary parts of all the four elements of the impedance tensor.

The structural penalty functional Φ_s is defined by

$$\Phi_s(\mathbf{m}, \mathbf{m}^{ref}) = (\mathbf{m} - \mathbf{m}^{ref})^T \mathbf{R}^T \mathbf{W}_m^2 \mathbf{R}(\mathbf{m} - \mathbf{m}^{ref}). \tag{3}$$

Here $\mathbf{m}^{ref}$ is a reference model, and $\mathbf{R}$ is a matrix of the first differences of the neighbouring model parameters. $\mathbf{W}_m$ is a weighting matrix for the model parameters, which may be determined by square roots of the integrated sensitivity matrix (Mehanee *et al.*, 1998).

The anisotropy penalty functional $\Phi_a(\mathbf{m})$ is defined according to Pain *et al.* (2003),

$$\Phi_a(\mathbf{m}) = \int_\Omega \begin{pmatrix} \ln\sigma_1 & \ln\sigma_2 & \ln\sigma_3 \end{pmatrix} \begin{pmatrix} 2 & -1 & -1 \\ -1 & 2 & -1 \\ -1 & -1 & 2 \end{pmatrix} \begin{pmatrix} \ln\sigma_1 \\ \ln\sigma_2 \\ \ln\sigma_3 \end{pmatrix} d\Omega, \tag{4}$$

the purpose of which is to make σ_1, σ_2 and σ_3 equal.

2.3 Minimization

Minimizing the objective functional (1) by the Gauss-Newton method leads to solving repeatedly, for a series of iteration steps, the following equation for the model perturbation $\delta\mathbf{m}$,

$$\left(\mathbf{S}^T\mathbf{W}_d^2\mathbf{S} + \lambda_s\mathbf{R}^T\mathbf{W}_m^2\mathbf{R} + \lambda_a\mathbf{A}\right)\delta\mathbf{m} = -\mathbf{S}^T\mathbf{W}_d^2\left[\mathbf{d}^{mod}(\mathbf{m}) - \mathbf{d}^{obs}\right] - \lambda_s\mathbf{R}^T\mathbf{W}_m^2\left[\mathbf{m} - \mathbf{m}^{ref}\right] - \lambda_a\mathbf{A}\mathbf{m}, \tag{5}$$

where $\mathbf{S}$ is the Jacobian matrix of sensitivities, which is obtained by the reciprocity method of sensitivity calculation presented in (Pek *et al.*, this volume). The matrix $\mathbf{A}$ is the extension matrix of the 3×3 symmetric matrix in eq. (4). The equation (5) is solved by the conjugate gradient least squares (CGLS) method (Björck, 1996). The obtained model perturbation $\delta\mathbf{m}$ is added to the current model parameter vector $\mathbf{m}$ to give the new model. With the updated model, the next iteration step is entered and (5) is solved again until a termination criterion is met.

3 Inversion results for synthetic data

This section presents inversion results for two synthetic data sets. The synthetic data sets are calculated with a finite element algorithm of Li (2002), whereas the inversion algorithm employs the finite difference algorithm of Pek & Verner (1997). Random noise was added to the computed impedance values, with a standard deviation of 2 percent.

3.1 Model 1

Fig. 1 shows the first test model, in which an anisotropic prism, with horizontal anisotropy only, is embedded into an isotropic homogeneous half-space with $\rho = 100$ Ωm. The inversion test uses the synthetic data at 13 sites along the surface and for 10 periods between 10 and 10^4 seconds, giving a total of 1040 data. The starting model for the inversion is an isotropic homogeneous half-space with the resistivity of 71 Ωm. The structural penalty parameter λ_s and the aniostropic penalty weight λ_a were chosen as 5 and 20, respectively. Fig. 2 shows an inversion solution for the synthetic data set generated from the model in Fig. 1. We can see that the anisotropic block is correctly reconstructed as to its position, and roughly as to the resistivity values and anisotropic angles. However, the α_s shows some artifacts outside the true anomalous zone, specifically α_s produces some symmetric 'wings' around the anomaly. The apparent resistivities and phases of the synthetic model (Fig. 1) and those of the inversion model (Fig. 2) are shown in Figs. 3 and 4, respectively. We can see a rather good agreement in all the four components of the apparent resistivity and phase.

3.2 Model 2

The second test model consists of two anisotropic prisms, again with horizontal anisotropy only, embedded in an isotropic homogeneous half-space (Fig. 5). The initial model for the inversion is again an isotropic homogeneous half-space, with the resistivity of 71 Ωm. The regularization parameters λ_s and λ_a were chosen as 5 and 20, respectively. Fig. 6. shows an inversion model obtained after 4 iterations. We can see that the two anisotropic blocks are good resolved as to their positions, and roughly also as to their resistivity values and angles. The apparent resistivities and phases from the synthetic model (Fig. 5) and those from the inversion model (Fig. 6) are shown in Figs. 7 and 8, respectively. We find good fits to both the apparent resistivities and phases.

4 Discussion and conclusions

We have presented the first test results of an inversion method for reconstructing anisotropic resistivity distribution in two dimensions from magnetotelluric fields. We have used the structural and anisotropic constraints to overcome the non-uniqueness of the solution of the inverse problem. The inversion method is demonstrated by using two simple synthetic models. Though the first results look promising, they present only a very basic step towards a practically working inverse procedure. The main purpose of the present contribution is just to demonstrate all the fundamental algorithmic items of the developed inverse procedure working together. There is still a lot of questions that have not been addressed yet, which specifically refers to various aspects of the regularization implementation (e.g., is it enough to regularize the structure and anisotropy simply by using the aggregated penalties (3) and (4), or is a separate, and maybe even adaptive regularization applied to individual parameters more appropriate, how to select the multiple regularization weights effectively, etc.), to questions of model smoothing and artifact suppression, and particularly to problems of the computational performance of the inverse algorithm. All these points are on the top of our present research activities.

5 Acknowledgments

This study is funded by the Deutsche Forschungsgemeinschaft (DFG) within the framework of the Collaborative Research Project SFB 267 *Deformation Processes in the Andes*. The participation of J.P. has been possible thanks to the financial support provided by the Grant Agency of the Academy of Sciences of the Czech Republic, contract No. IAA3012401, as well as by the Geophysical Inst., Acad. Sci. Czech Rep., contract No. AV0Z3012916.

References

[1] Bahr, K. & Simpson, F., 2002. Electrical anisotropy below slow- and fast-moving plates: Paleoflow in the upper mantle? *Science*, **295**, 1270–1272.

[2] Björck, Å, 1996. *Numerical methods for least squares problems*, SIAM, Philadelphia.

[3] Eisel, M. & Haak, V., 1999. Macro-anisotropy of the electrical conductivity of the crust: A magnetotelluric study from the German Continental Deep Drilling site (KTB), *Geophys. J. Int.*, **136**, 109–122.

[4] Lezaeta, P. & Haak, V., 2003. Beyond magnetotelluric decomposition: Induction, current channeling, and magnetotelluric phases over 90 degrees, *J. Geophys. Res.–SE*, **108**, Art. No. 2305.

[5] Li, Y., 2002. A finite-element algorithm for electromagnetic induction in two-dimensional anisotropic conductivity structures, *Geophys. J. Int.*, **148**, 389-401.

[6] Mareschal, M., Kellett, R. L., Kurtz, R. D., Ludden, J. N., Ji, S. & Bailey, R. C., 1995. Archean cratonic roots, mantle shear zones and deep electrical anisotropy, *Nature*, **375**, 134–137.

[7] Mehanee, S., Golubev, N. & Zhdanov, M., 1998. Weighted regularized inversion of magnetotelluric data, in *1998 SEG Expanded Abstracts*.

[8] Pain, C., Herwanger, J. V., Saunders, J. H., Worthington, M. H. & Oliveora, C. R. E., 2003. Anisotropic resistivity inversion, *Inverse Problems*, **19**, 1081–1111.

[9] Pek, J. & Verner, T., 1997. Finite-difference modelling of magnetotelluric fields in two-dimensional anisotropic media, *Geophys. J. Int.*, **128**, 505–521.

[10] Pek, J. & Santos, F. A. M., 2001. Magnetotelluric inversion for anisotropic conductivities, in Protokoll Kolloquium *Elektromagnetische Tiefenforschung*, Burg Ludwigstein 1.-15. 10. 2001.

[11] Pek, J., Santos, F. A. M. & Li.,Y., 2004. Parametric sensitivities for 2-D anisotropic magnetotelluric model, in this volume.

[12] Simpson, F., 2001. Resistance to mantle flow inferred from the electromagnetic strike of the Australian upper mantle, *Nature*, **412**, 632–635.

[13] Weckmann, U., Ritter, O. & Haak, V., 2003. A magnetotelluric study of the Damara Belt in Namibia 2. MT phases over 90 degrees reveal the internal structure of the Waterberg Fault/Omaruru Lineament, *Physics of the Earth and Planetary Interiors*, **138**, 91–112.

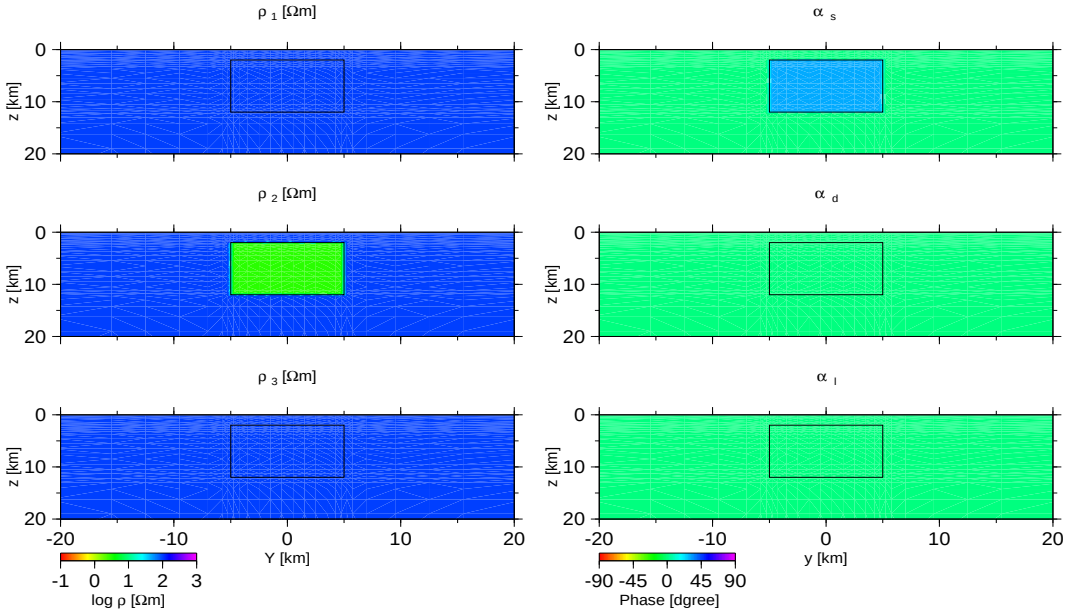

Figure 1: The synthetic model 1. Anisotropic prism is embedded into an isotropic homogeneous half-space of 100 Ωm. The principal resistivities and anisotropy directions within the anomaly are $\rho_1/\rho_2/\rho_3 = 100/10/100$ Ωm and $\alpha_s = 30°$, $\alpha_d = \alpha_l = 0°$.

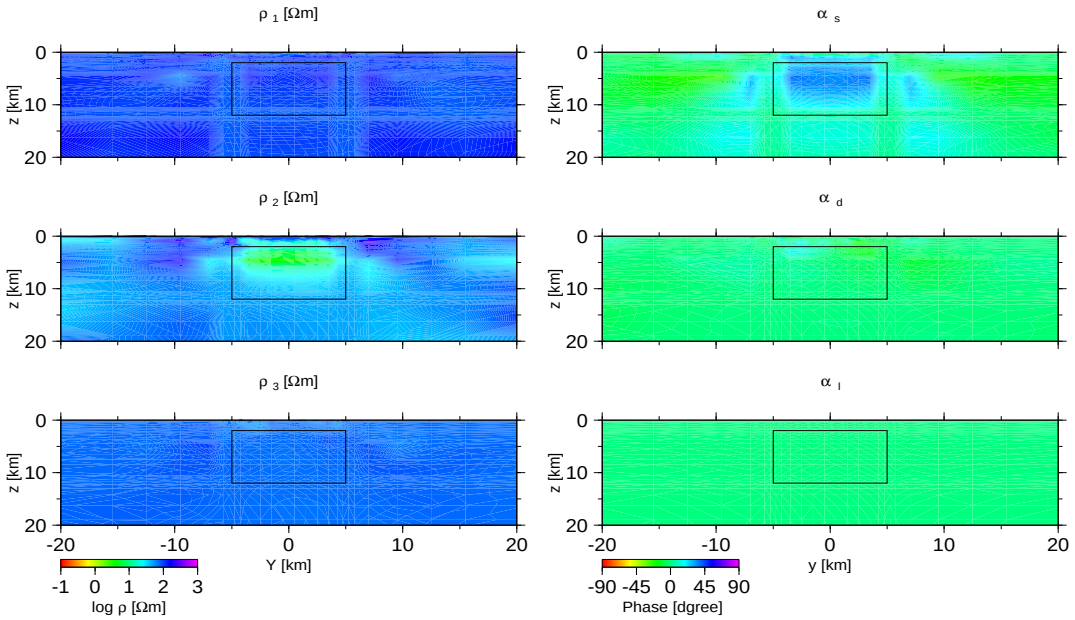

Figure 2: Inversion model for the synthetic data set generated from the model in Fig. 1.

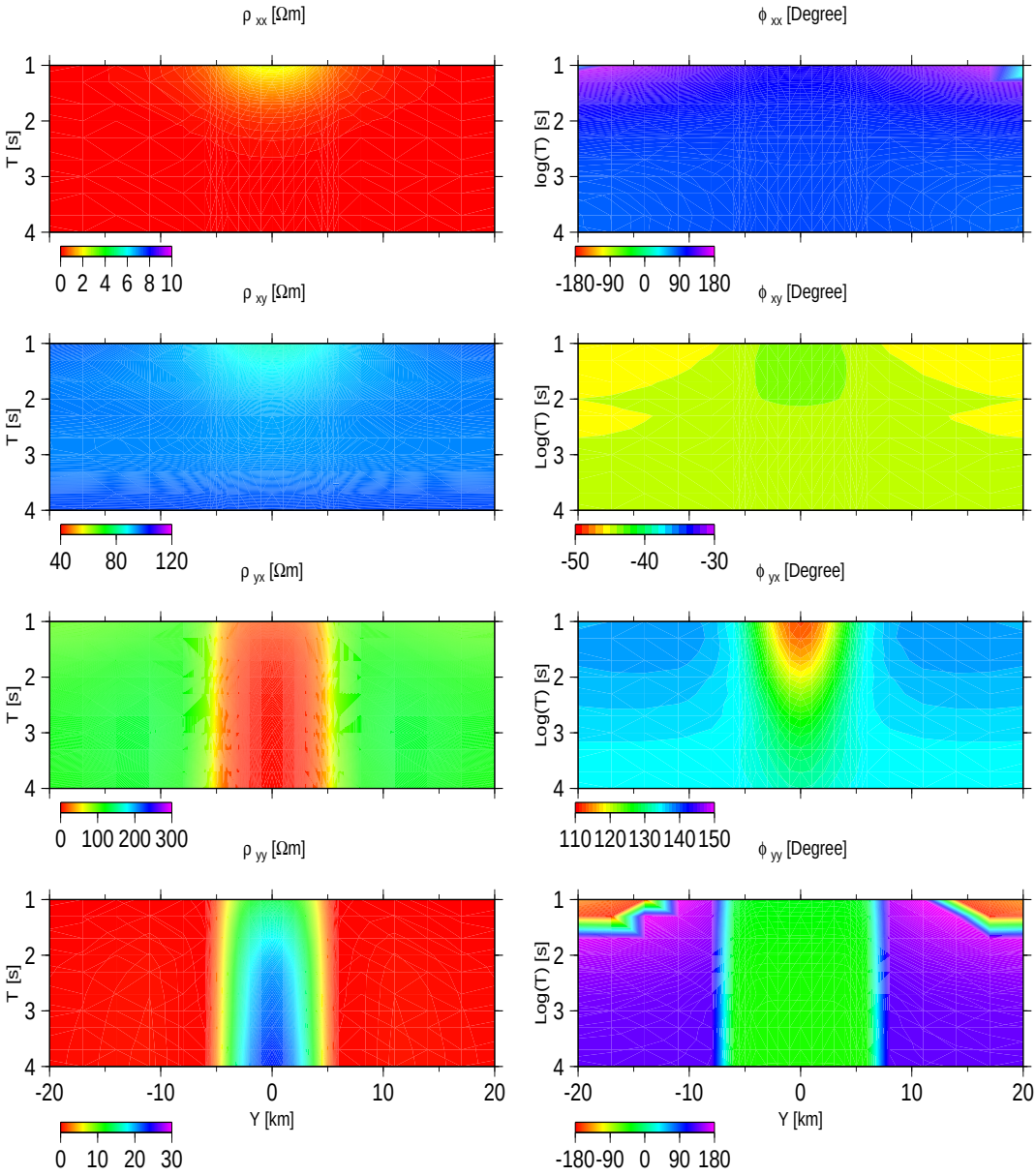

Figure 3: The apparent resistivities and phases from the model shown in Fig. 1.

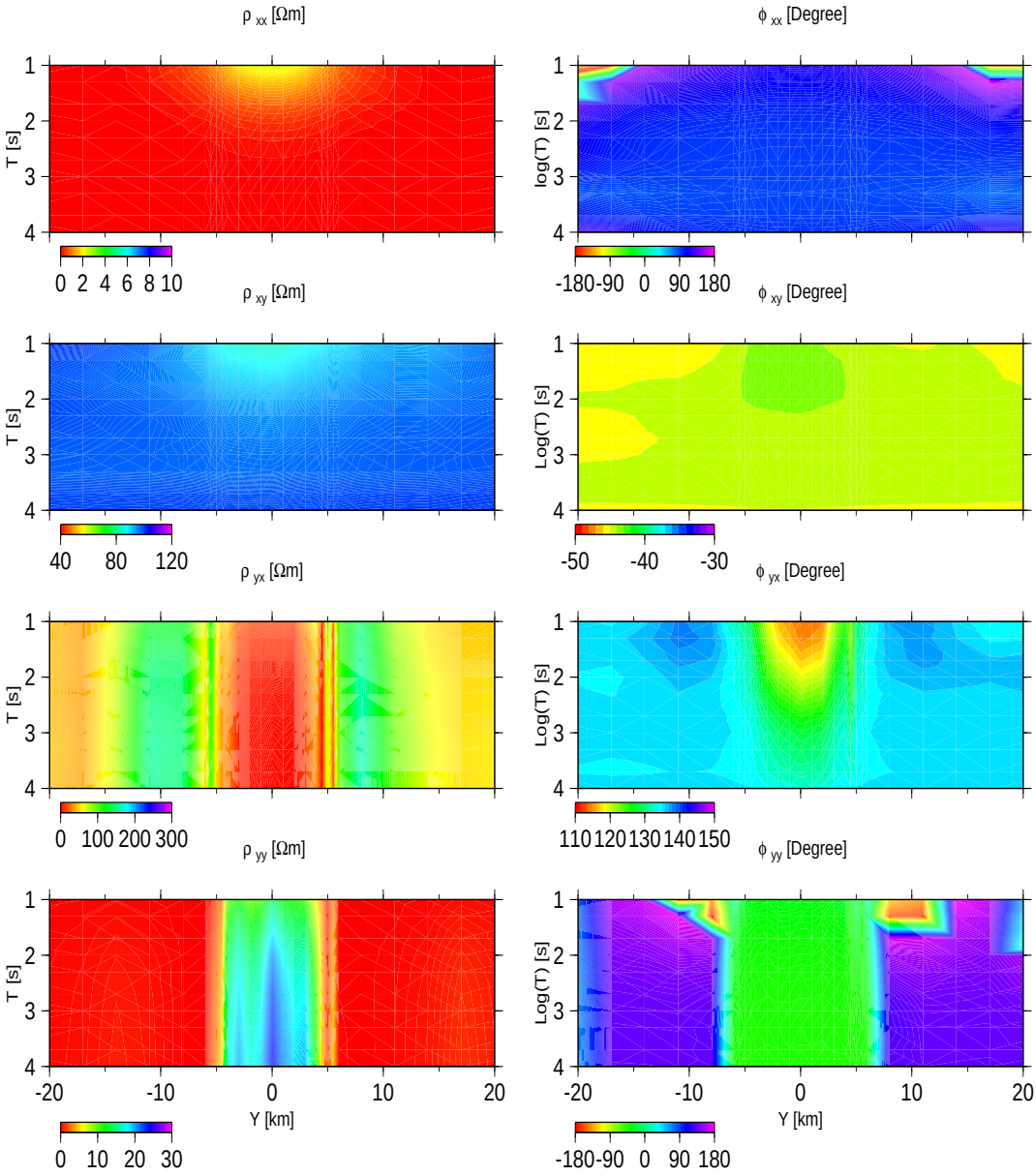

Figure 4: The apparent resistivities and phases from the inversion model shown in Fig. 2.

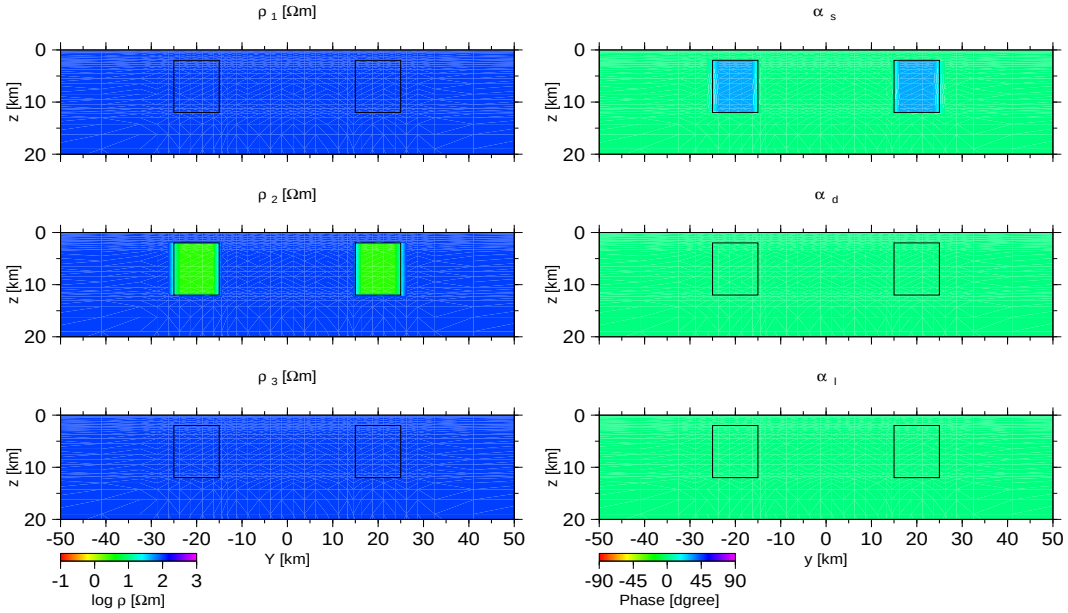

Figure 5: The synthetic model 2. It consists of two anisotropic prisms with horizontal anisotropy.

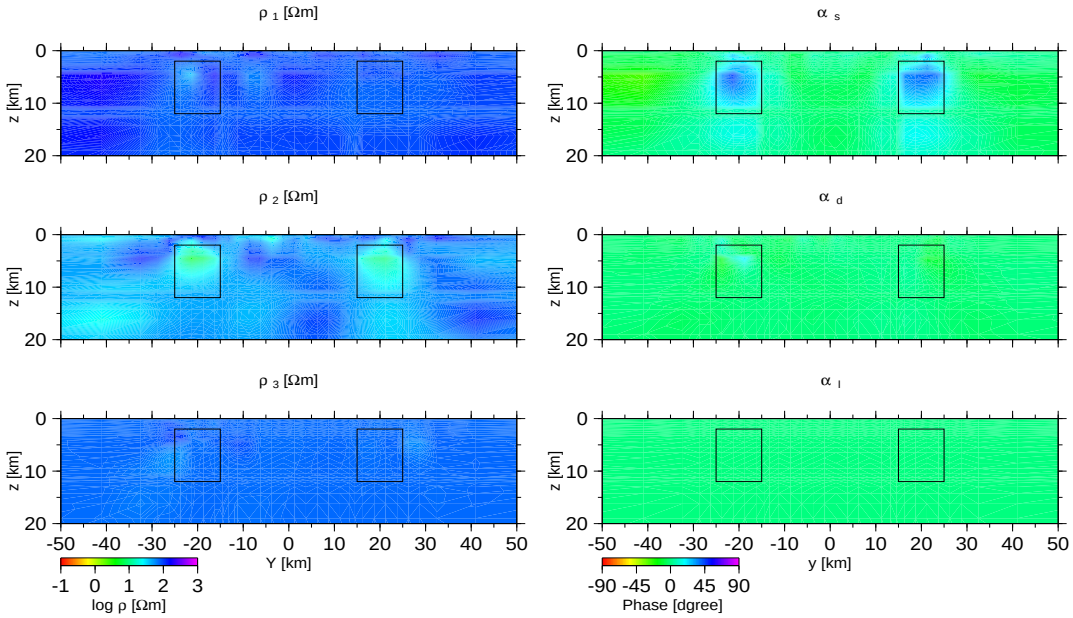

Figure 6: Inversion model for the synthetic data set generated from the model in Fig. 5.

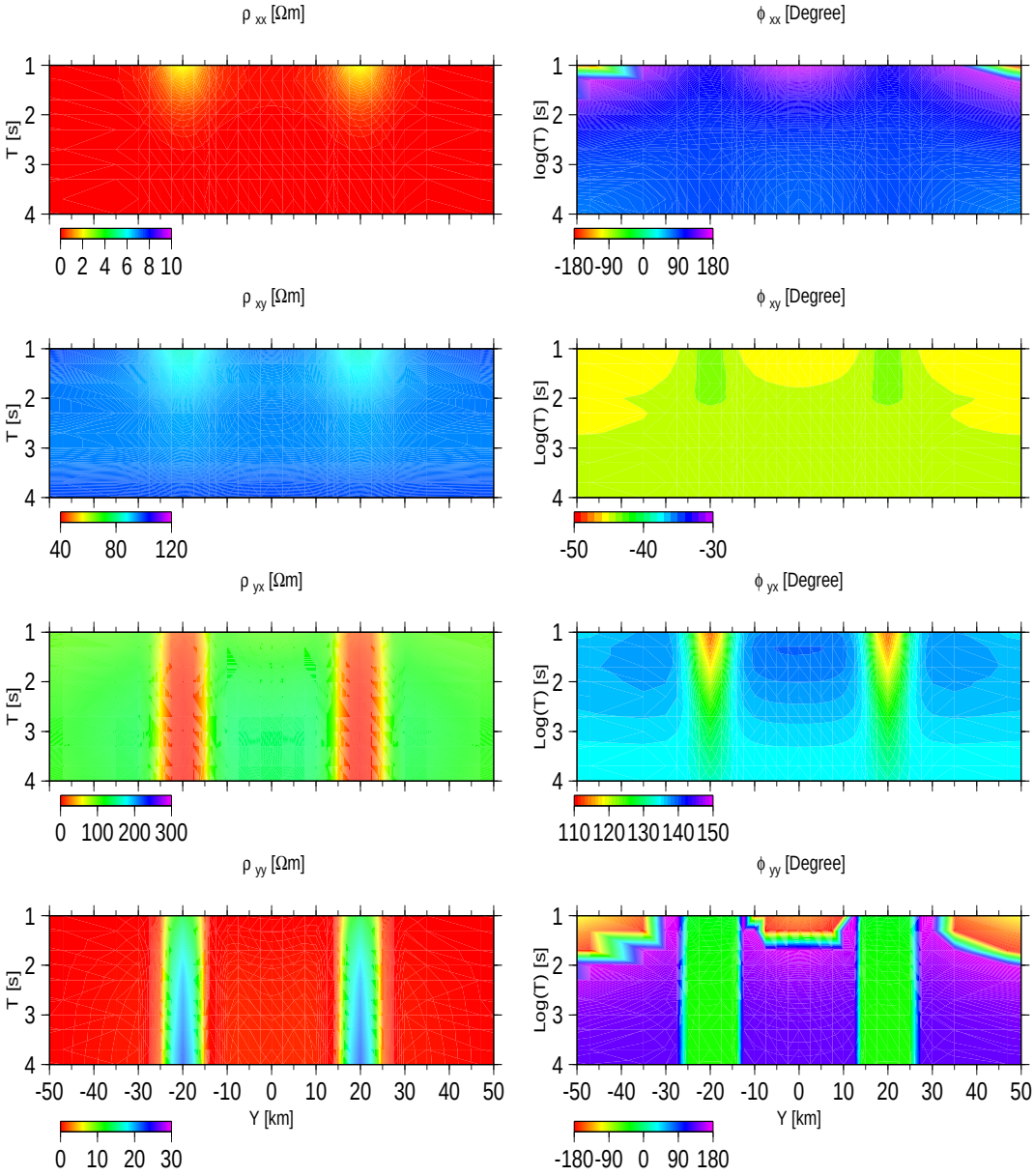

Figure 7: The apparent resistivities and phases from the synthetic model shown in Fig. 5.

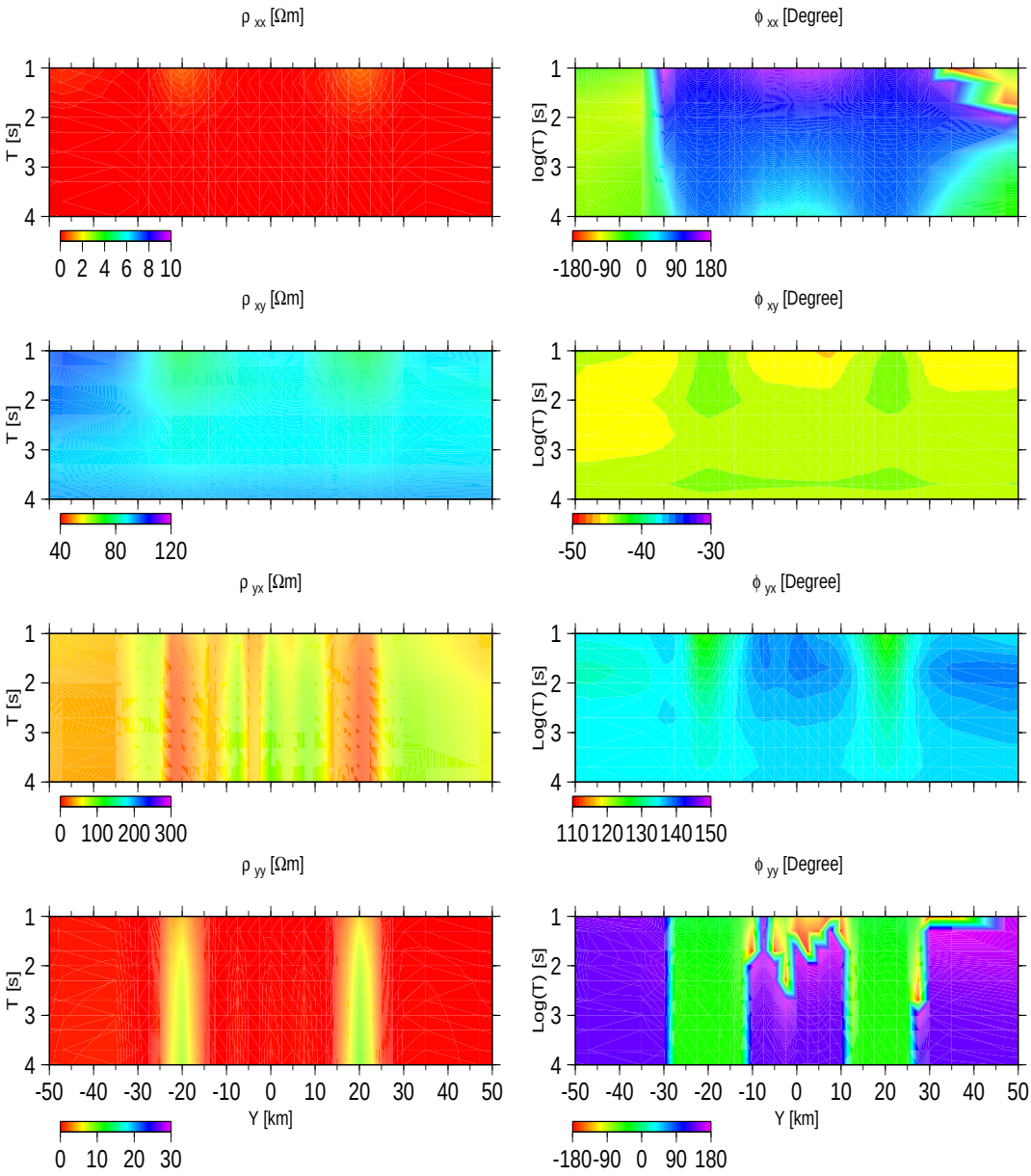

Figure 8: The apparent resistivities and phases from the inversion model shown in Fig. 6.